Articles

Synthesis and Characterization of Glycomethacrylate Hybrid Stars from Silsesquioxane Nanoparticles

Sharmila Muthukrishnan,[†] Felix Plamper,[†] Hideharu Mori,[‡] and Axel H. E. Müller*,[†]

Makromolekulare Chemie II and Bayreuther Zentrum für Kolloide und Grenzflächen, Universität Bayreuth, D-95440 Bayreuth, Germany, and Department of Polymer Science and Engineering, Faculty of Engineering, Yamagata University, 4-3-16, Jonan, Yonezawa, 992-8510, Japan

Received September 6, 2005; Revised Manuscript Received October 13, 2005

ABSTRACT: A silsesquioxane nanoparticle based macroinitiator of ca. 58 functions was synthesized and characterized using ^{1}H NMR, MALDI-TOF MS, and elemental analysis. The macroinitiator was used to synthesize glycomethacrylate stars with approximately 25 arms of different lengths using 3-*O*-methacryloyl-1,2:5,6-di-*O*-isopropylidene-α-D-glucofuranose (MAIGlc) as the monomer via atom transfer radical polymerization (ATRP). Well-defined glycostars could be synthesized by restricting the polymerization to low conversion. The molecular weights of the star polymers were determined using gel permeation chromatography (GPC) with viscosity and multiangle light scattering (MALS) detectors. To determine the efficiency of the initiating sites, the arms were cleaved from the core by solvolysis with sodium methoxide and thoroughly characterized, indicating that ca. 25 arms per star had been synthesized. The morphology of the glycostars was visualized using scanning force microscopy (SFM) and field emission scanning electron microscopy (FE-SEM). Deprotection of the isopropylidene groups resulted in water-soluble stars that were characterized using SFM, SEM, asymmetric flow field-flow fractionation (AF-FFF), dynamic light scattering (DLS), cryogenic transmission electron microscopy (cryo-TEM), and bright-field transmission electron microscopy (TEM).

Introduction

Branched structures have been the subject of continuing interest in polymer chemistry. Branched polymers in comparison to their linear analogues with identical molecular weights offer lower melt and solution viscosities.[1,2] They possess different hydrodynamic properties and higher degrees of chain end functionality compared to linear polymers of similar composition. Precise architectural control in polymers is essential because it affects their properties and morphology. Among the branched structures, star polymers are architecturally interesting since each molecule has only one branch point. The synthesis of well-defined stars has always been a challenging task. There are two main methods to obtain star polymers: either by linking a given number of linear chains to a central core ("arm-first" method)[3,4] or by growing branches from an active core ("core-first" method).[5,6] To obtain stars with a precise number of arms by using the core-first methodology, it is essential to use structurally well-defined plurifunctional initiators.

To obtain well-defined stars, it is essential that a controlled polymerization technique be used that maintains chain functionality. There are different techniques such as living cationic,[7,8] anionic,[9] and group transfer metathesis polymerization[10,11] to obtain well-defined stars, but all require strenuous methods of reagent purification and are only useful for a limited range of monomers. The development of controlled/"living" radical polymerization has opened up a potentially wide path to well-defined macromolecules.[12−14] Among the various controlled/"living" radical polymerization techniques, atom transfer radical polymerization (ATRP) provides control over chain length and chain functionality by maintaining a very low steady-state concentration of active growing chains that are in dynamic equilibrium with the so-called dormant species. There are several reports on ATRP-based synthesis of stars of different arm numbers using organic initiators and different transition metal catalysts.[15−19] There has been growing attention and interest in the synthesis of star polymers initiated by inorganic cores.[18] Recently, the successful synthesis of organic/inorganic hybrid stars from an octafunctional cubic silsesquioxane via ATRP of methyl methacrylate has been reported.[20] This is due to the general interest of combining the potential application of hybrid materials with the facility with which branched polymers can be processed.[21]

Here, we demonstrate the use of a novel silsesquioxane nanoparticle based macroinitiator for ATRP with approximately 58 initiating functions to initiate the polymerization of a bulky sugar-carrying methacrylate monomer, 3-*O*-methacryloyl-1,2:5,6-di-*O*-isopropylidene-α-D-glucofuranose (MAIGlc) and to describe the condi-

* To whom correspondence should be addressed. Phone:+49 (921) 55-3399. Fax: +49 (921) 55-3393. E-mail: Axel.Mueller@uni-bayreuth.de.
[†] Universität Bayreuth.
[‡] Yamagata University.

10.1021/ma051949e CCC: $30.25
Published on Web 11/19/2005

Scheme 1. General Route to Synthesis of Glycopolymer/Silsesquioxane Hybrid Stars

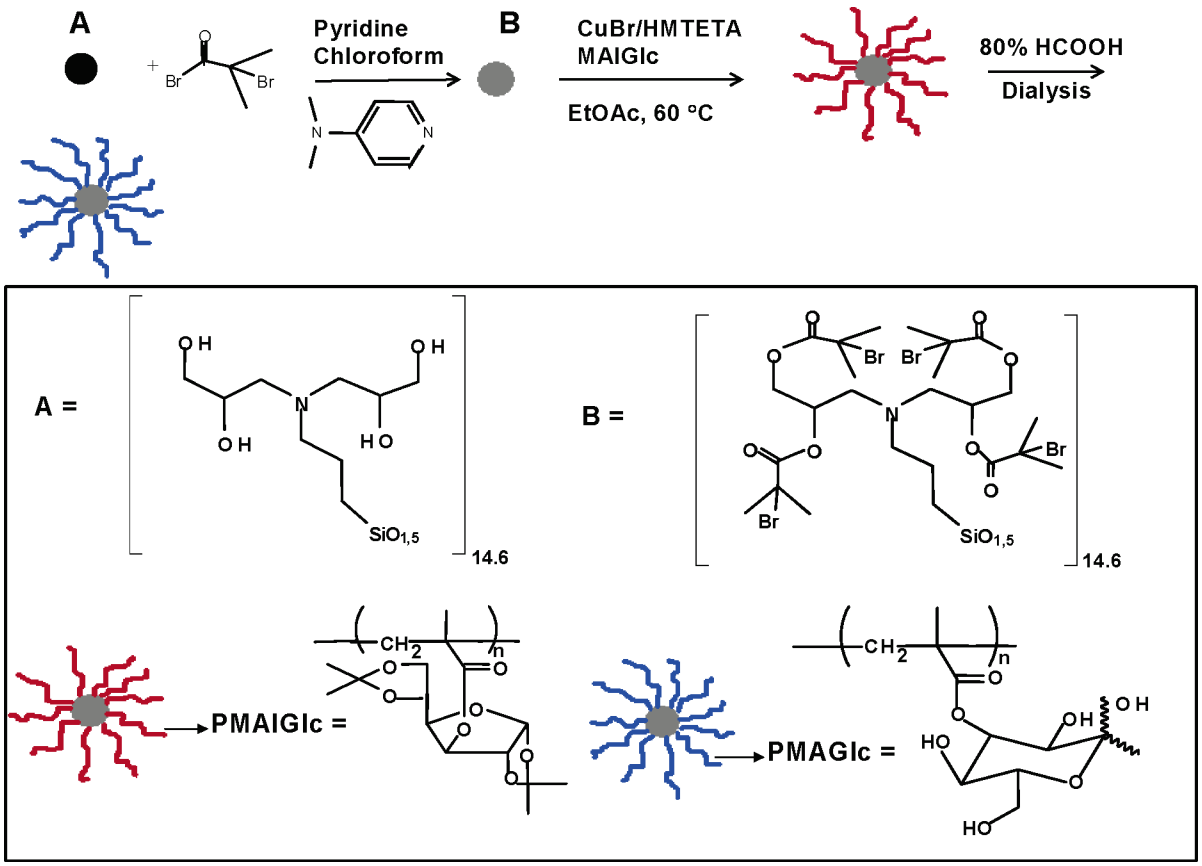

tions best suited to the synthesis of well-defined glycostars. In recent years there has been increasing attention paid to the synthesis of glycopolymers due to their high hydrophilicity and water solubility. They can be used as efficient tools to investigate carbohydrate-based interactions and to understand nature's multivalent processes.[22] They are of main interest with respect to very specialized applications in biochemical and biomedical fields, such as molecular recognition processes[23] and drug delivery systems.[24]

Controlled/"living" radical polymerization has proved to be a very facile approach for well-defined and controlled synthesis of glycopolymers.[25−27] As a part of our continuous efforts to develop branched glycopolymers having controlled architectures, here we report on the synthesis of well-defined glycostars using a "core-first" approach via ATRP. We have very recently reported the synthesis and structural characterization of functional silsesquioxane-based nanoparticles.[28,29] In this paper, these silsesquioxane nanoparticles are modified into ATRP macroinitiators with approximately 58 functions and used for the synthesis of glycopolymer/nanoparticle hybrids. Such organic−inorganic hybrid nanoparticles have attracted a great deal of attention due to their wide range of applications in optics, engineering, and biosciences. To the best of our knowledge, this is the first paper on employing silsesquioxane nanoparticle based macroinitiators for the synthesis of well-defined glycopolymer−inorganic hybrid stars. The synthetic route leading to glycostars is shown in Scheme 1.

Experimental Section

Materials. CuBr (95%, Aldrich) was purified by stirring overnight in acetic acid. After filtration, it was washed with ethanol and ether and then dried. 1,1,4,7,10,10-Hexamethyltriethylenetetramine (HMTETA, 97%, Aldrich) was distilled and degassed before use. 3-*O*-Methacryloyl-1,2:5,6-di-*O*-isopropylidene-D-glucofuranose (MAIGlc) was synthesized by the reaction of 1,2:5,6-di-*O*-isopropylidene-D-glucofuranose and methacrylic anhydride in pyridine and purified by vaccum distillation as reported by us recently.[30] 2-Bromo-2-methylpropionyl bromide (98%, Aldrich) and 4-(*N*,*N*-dimethylamino)-pyridine (99%, Aldrich) were used as received without further purification. The synthesis of the functional silsesquioxane nanoparticles with 3-bis(2,3-dihydroxypropyl)aminopropyl functions by acidic condensation of the corresponding triethoxysilane was described earlier.[28,29]

Synthesis of Silsesquioxane-Based Macroinitiator. The functional silsesquioxane nanoparticles (10 g; 0.155 mol of hydroxy groups) were dried thoroughly in a vacuum oven at 80 °C for 3 h before use. Pyridine (60 mL) and chloroform (100 mL) were added to a round-bottom flask containing nanoparticles. To the above solution was added one spatula of 4-(*N*,*N*-dimethylamino)pyridine, and then it was cooled with ice. 2-Bromo-2-methylpropionyl bromide (41 g; 0.178 mol; 22 mL) was added dropwise slowly until the mixture changed to yellow. The mixture was stirred for 2 days. Then the brown suspension was diluted with diethyl ether (two liquid phases) and extracted twice with cold water. The yellow organic phase was washed twice with 5 wt % NaOH. Finally, the organic layer was dried with $MgSO_4$ and the solvent was removed under reduced pressure. The product was then freeze-dried from dioxane (17 g; yield 51%). It was further purified by dialysis from tetrahydrofuran (THF) (Spectra Pore; MWCO 1000 Da). After 2 days the solution was concentrated, freeze-dried from dioxane, and dried in the vacuum oven (40 °C; 4 h). ^{1}H NMR ($CDCl_3$): 0.3−0.8 (−CH_2 in the α position to the silicon atom), 1.3−1.7 (−CH_2 in the β position to the silicon atom), 1.8−2.0 (−CH_3 adjacent to the bromine atom), 2.2−3.0 (−CH_2 in the α position to the N atom), and 3.9−5.3 (−CH_2 and −CH in the α position to the O atom). The molecular weight and polydispersity index (PDI) for the modified nano-

Table 1. Synthesis and Characterization of Silsesquioxane-Based Glycomethacrylate Stars via ATRP[a]

glycostar	$[M]_0/[I]_0$	time (min)	conv[b] (%)	$10^{-4}M_{n,calcd}$[c]	$10^{-4}M_{n,GPC}$[d] (PDI)	$10^{-4}M_{n,GPC-VISCO}$[e] (PDI)	$10^{-4}M_{n,GPC/MALS}$[f] (PDI)	$DP_{n,arm,calcd}$[g]
1	100	10	16.0	30.4	11.8 (1.09)	24.5 (1.25)	24.9 (1.12)	13
2	300	15	5.0	28.5	9.2 (1.08)	25.6 (1.25)	26.4 (1.12)	14
3	300	25	8.0	45.7	16.0 (1.12)	41.6 (1.17)	43.6 (1.20)	23
4	600	25	6.0	68.4	23.2 (1.12)	60.1 (1.26)	66.0 (1.12)	35

[a] Solution polymerization in ethyl acetate (50 wt % to MAIGlc) at 60 °C at constant $[I]_0:[CuBr]_0:[HMTETA]_0 = 1:0.5:0.5$. [b] Determined by ^{1}H NMR. [c] Calculated assuming 100% initiation site efficiency of the silsesquioxane-based macroinitiator. [d] Determined by GPC using THF as eluent with PtBMA standards. [e] Determined by GPC/viscosity measurement. [f] Determined by GPC/MALS measurement. [g] Calculated from $M_{n,GPC/MALS}$ assuming 100% initiation site efficiency.

particles as determined by MALDI-TOF MS were $M_n = 10\,500$ and $M_w/M_n = 1.25$, respectively.

Elemental Analysis: 37.44 wt % Br (expected, 37.41); 1.70 wt % N (expected, 1.64); 3.38 wt % Si (expected, 3.29).

Polymerizations. All polymerizations were carried out in a round-bottom flask sealed with a plastic cap. A representative example for the synthesis of glycostars is as follows: To a round-bottom flask containing CuBr (3.5 mg, 0.025 mmol), MAIGlc (5.0 g, 15.24 mmol) in ethyl acetate (5.0 g, 50 wt %) was added the silsesquioxane-based macroinitiator (10.1 mg, 0.050 mmol) (see Table 1); the mixture was stirred for 5 min to dissolve the macroinitiator completely. Then HMTETA (5.6 mg, 0.025 mmol) was added to this mixture and the color changed to green, indicating the start of the polymerization. The flask was then placed in an oil bath at 60 °C for 25 min. Monomer conversion, as detected by ^{1}H NMR, was 8%. The content in the flask was viscous even at such a low conversion and was then dissolved in THF. The solution was passed through a silica column, and the polymer was precipitated from THF into methanol two times. Then it was again precipitated in petroleum ether twice to remove the unreacted monomer completely. Finally, the product was freeze-dried from dioxane and dried under vacuum at room temperature. The polymer had $M_n = 16.0 \times 10^4$ and $M_w/M_n = 1.12$ according to conventional gel permeation chromatography (GPC) using PtBMA calibration, $M_n = 41.6 \times 10^4$ and $M_w/M_n = 1.17$ according to GPC/viscosity using universal calibration, and $M_n = 43.6 \times 10^4$ and $M_w/M_n = 1.20$ according to GPC/multiangle light scattering (MALS) measurement. The resulting polymer was completely soluble in THF, chloroform, and dioxane but insoluble in methanol, acetone, and water.

Solvolysis of the Glycostars. Arm cleavage was achieved via base-catalyzed transesterification in methanol similar to that adopted for the solvolysis of glycocylindrical brushes.[31,32] The polymer (10 mg) was dissolved in THF in a capped vial. Methanol was added until the polymer was precipitated, and then sodium methoxide (25% in methanol, 4−5 drops) was added. The capped vial was then placed in an oil bath and kept at 90 °C for 3 days. Then, the solution was cooled and stirred for 2 h in the presence of a cationic ion-exchange resin (Dowex MSC-1). The solution was decanted and evaporated to yield cleaved arms. The molecular weight of the resulting product was analyzed using conventional GPC and GPC/MALS measurements.

Deprotection. The transformation of protected glycostars into water-soluble ones with poly(3-*O*-methacryloyl-α,β-D-glucopyranose) (MAGlc) arms was achieved under mild acidic condition.[30] The polymer (50 mg) was dissolved in 80% formic acid (12 mL) and stirred for 48 h at room temperature. Then 5 mL of water was added and it was stirred for another 3 h. The solution was dialyzed using a Spectra/Por dialysis tube (MWCO 1000) against Millipore water for 2 days. The resulting polymer was freeze-dried from water and dried under vacuum. The deprotected polymer was obtained as a white powder that was soluble in water and methanol, but insoluble in THF and acetone.

Characterization. The apparent molecular weights of the stars and cleaved arms were characterized by conventional GPC using THF as eluent at a flow rate of 1.0 mL/min at room temperature: column set, 5 μm PSS SDV gel, 10^2, 10^3, 10^4, and 10^5 Å, 30 cm each; detectors, Waters 410 differential refractometer and Waters photodiode array detector operated at 254 nm. Narrow PtBMA and poly(methyl methacrylate) (PMMA) standards (PSS, Mainz) were used for the calibration of the column set. GPC with a multiangle light scattering detector (GPC/MALS) and GPC with a Viscotek viscosity detector H 502B (GPC/viscosity) were used to determine the absolute molecular weights of the stars and of the arms cleaved by solvolysis. THF was used as eluent at a flow rate of 1.0 mL/min: column set, 5 μm PSS SDV gel, 10^3, 10^5, and 10^6 Å, 30 cm each; detectors, Shodex RI-71 refractive index detector and Wyatt DAWN DSP-F MALS detector equipped with a 632.8 nm He−Ne laser. The refractive index increments in THF solution of the glycostar and cleaved arms at 25 °C were determined to be $dn/dc = 0.066$ and 0.065 mL/mg, respectively, using a PSS DnDc-2010/620 differential refractometer. The refractive index increment in water solution of the deprotected glycostar at 25 °C was determined to be 0.146 mL/mg. For GPC/viscosity the universal calibration principle was used. Linear PMMA standards (PSS, Mainz) were used to construct the universal calibration curve. ^{1}H NMR was recorded with a Bruker AC-250 instrument at room temperature. Fourier transform infrared (FT-IR) spectra were recorded on a Bruker Equinox 55 spectrometer. The elemental analyses were performed by IIse Beetz Mikroanalytisches Laboratorium (Kulmbach).

MALDI-TOF mass spectrometry was performed on a Bruker Reflex III instrument equipped with a 337 nm N_2 laser in the reflector mode and 20 kV acceleration voltage. 2,5-Dihydroxybenzoic acid (Aldrich, 97%) was used as a matrix for molecular weight determination of the silsesquioxane initiator (mass ratio DHB:initiator 10:1; linear mode). Overlap with signals of matrix or low molecular weight compounds was resolved by Lorentzian fit in the undisturbed region, as a Gaussian fit was shown to be less suitable for proper alignment with the measured signal.

Asymmetric flow field-flow fractionation (AF-FFF) was accomplished for the deprotected glycostar on a Postnova HRFFF-10000 system equipped with RI, UV, and multiangle light scattering (Wyatt DAWN EOS, $\lambda = 632.8$ nm) detectors: dimension of the channel, 0.35 mm; cutoff molecular weight of the membrane 5 kDa; injection volume, 20 μL; constant cross-flow gradient, 1.5 mL/min within 30 min; laminar flow out, 0.6 mL/min; eluent, water with 25 mM sodium nitrate and 200 ppm sodium azide; sample concentration, 0.5 g/L.

Dynamic light scattering (DLS) was performed on an ALV DLS/SLS-SP 5022F compact goniometer system with an ALV 5000/E correlator and a He−Ne laser ($\lambda = 632.8$ nm). Prior to the light scattering measurements the sample solutions were filtered using Millipore Teflon filters with a pore size of 0.45 μm. The measured intensity correlation functions were subjected to CONTIN analysis. Apparent hydrodynamic radii of the glycostars were calculated according to the Stokes−Einstein equation.

The samples for scanning force miscroscopy (SFM) measurements were prepared by spin-coating from dilute (8 mg/L) solutions of glycostars in tetrahydrofuran or methanol/water (1/1, volume ratio) mixtures onto freshly cleaved mica surfaces. The SFM images were taken with a Digital Instruments Dimension 3100 microscope operated in tapping mode (free amplitude of the cantilever ≈ 30 nm, set-point ratio ≈ 0.98, tip radius ∼ 20 nm).

The samples for field emission scanning electron microscopy (FE-SEM) measurements were prepared by spin-coating from dilute (8 mg/L) solutions of glycostars in tetrahydrofuran or methanol/water (1/1, volume ratio) mixtures onto polished

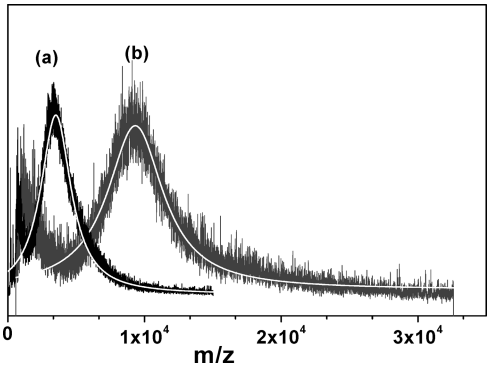

Figure 1. MALDI-TOF mass spectra of (a) silsesquioxane nanoparticles and (b) silsesquioxane-based macroinitiator. The lines represent Lorentzian fits.

silicon wafers. These samples were directly characterized by using a LEO 1530 Gemini microscope (acceleration voltage, 1.0 kV).

Bright-field transmission electron microscopy (TEM) was performed using a Zeiss electron microscope (CEM 902) operated at 80 kV. The samples were prepared by negative staining with uranyl acetate on carbon-coated Cu grids from dilute (10 mg/L) water solutions according to the standard procedure.[33] For cryogenic transmission electron microscopy (cryo-TEM) studies, a drop of the sample was put on an untreated bare copper TEM grid (600 mesh, Science Services, München, Germany), where most of the liquid was removed with blotting paper, leaving a thin film stretched over the grid holes. The specimens were instantly shock frozen by rapid immersion into liquid ethane and cooled to approximately 90 K by liquid nitrogen in a temperature-controlled freezing unit (Zeiss Cryobox, Zeiss NTS GmbH, Oberkochen, Germany). The temperature was monitored and kept constant in the chamber during all the sample preparation steps. After freezing the specimens, the remaining ethane was removed using blotting paper. The specimen was inserted into a cryo-transfer holder (CT3500, Gatan, München, Germany) and transferred to a Zeiss EM922 EF-TEM. Examinations were carried out at temperatures around 90 K at an acceleration voltage of 200 kV. Zero-loss filtered images ($\Delta E = 0$ eV) were taken under reduced dose conditions (100−1000 electrons/nm^2). All images were registered digitally by a bottom-mounted CCD camera system (Ultrascan 1000, Gatan) combined and processed with a digital imaging processing system (Gatan Digital Micrograph 3.9 for GMS 1.4).

Results and Discussion

Synthesis and Characterization of the Silsesquioxane Nanoparticle Based Macroinitiator. We have very recently reported the synthesis and structural determination of functional silsesquioxane nanoparticles (see Scheme 1).[28,29] The molecular weight and PDI of the nanoparticles are $M_n = 3760$ and $M_w/M_n = 1.21$ as determined by MALDI-TOF MS. These nanoparticles were found to consist of complete and incomplete cagelike structures with Si−O−Si and Si−O−C bonds.[28] The average particle size is 2.7 nm as determined by TEM. Since the molecular weight of a unit with one Si atom is 258.3, the particles contain approximately 14.6 Si atoms or 58 hydroxyl functions. The standard deviation of the MALDI-TOF MS distribution (Figure 1) is 31%; thus the particles have 58 ± 18 hydroxyl functions.

These silsesquioxane nanoparticles were transformed to ATRP macroinitiators with approximately 58 initiating functions by the esterification reaction with 2-bromoisobutyryl bromide. Figure 2 represents the ^{1}H NMR spectra of the silsesquioxane-based nanoparticles and macroinitiator. The characteristics peaks of the macroinitiator are clearly seen at 0.3−0.8 (CH_2 in the α position to the silicon atom), 1.3−1.7 (CH_2 in the β position to the silicon atom), 1.8−2.0 ($-CH_3$ adjacent to the bromine atom), 2.2−3.0 (CH_2 in the α position to the N atom), and 3.9−5.3 (CH_2 and CH in the α position to the O atom), respectively, indicating the successful synthesis of the macroinitiator.

Figure 3 shows the FT-IR spectra of the nanoparticles and the macroinitiator. In the case of nanoparticles, there is a broad absorption band for the hydroxyl functionality from 3000 to 3800 cm^{-1} with a maximum at 3400 cm^{-1}. In addition, a sharp peak between 2840 and 2940 cm^{-1} is seen, which is due to the C−H

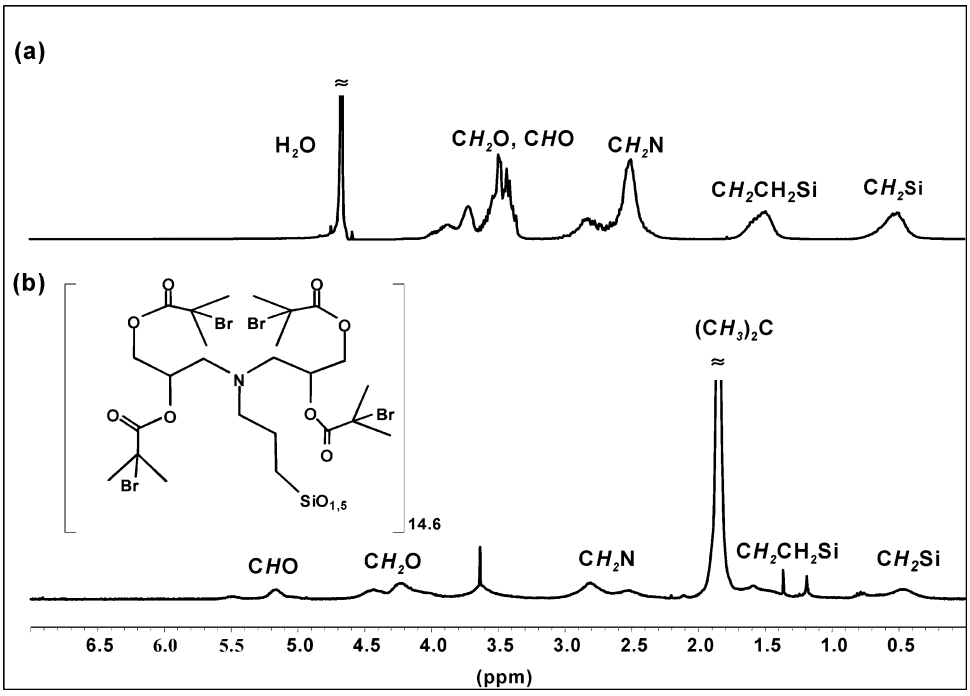

Figure 2. ^{1}H NMR spectra of (a) silsesquioxane-based nanoparticles (D_2O) and (b) silsesquioxane-based macroinitiator ($CDCl_3$).

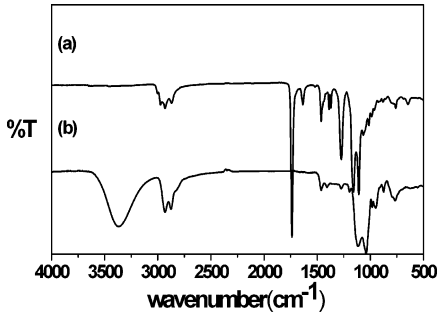

Figure 3. FT-IR spectra of (a) silsesquioxane-based macroinitiator and (b) silsesquioxane nanoparticles.

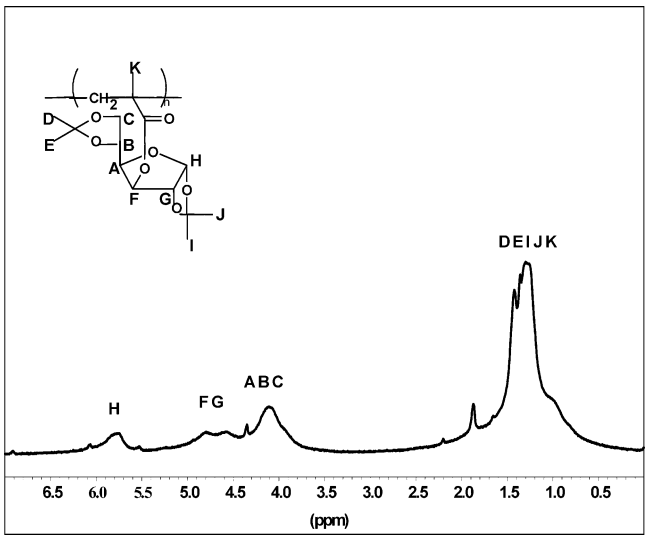

Figure 4. ^{1}H NMR spectrum ($CDCl_3$) of glycostar 4, poly(MAIGlc).

stretching vibration in the alkyl chain on the nanoparticles, and also a strong absorption band around 1030−1150 cm^{-1} resulting from Si−O−Si stretching is observed. In the case of the silsesquioxane-based macroinitiator, the disappearance of the broad absorption band of OH functionality around 3000−3800 cm^{-1} and also the appearance of a sharp peak at 1740 cm^{-1} resulting from the carbonyl functionality indicate the successful synthesis of the macroinitiator.

The macroinitiator was further investigated by MALDI-TOF MS and elemental analysis. The molecular weight and PDI of the modified nanoparticles are M_n = 10 200 and M_w/M_n = 1.25 (Figure 1). The molecular weight is lower than the calculated one ($M_{n,calcd}$ = 12 500). Since FT-IR indicates full conversion of hydroxyl functions to α-bromoesters, we attribute the difference to the loss of HBr molecules in the ionization procedure, which is a common observation for bromoesters.[19] The atomic composition of the silsesquioxane-based macroinitiator determined by elemental analysis is for Br, 37.44; for N, 1.70; and for Si, 3.38 (calcd: Br, 37.41; N, 1.64; Si, 3.29); respectively. The agreement between experimental and calculated values indicates the successful synthesis of the silsesquioxane-based macroinitiator of approximately 58 functions.

Synthesis and Characterization of Glycomethacrylate Stars. We have recently reported that CuBr/HMTETA is one of the best catalyst systems for the hompolymerization of MAIGlc to obtain linear poly(MAIGlc)s with narrow molecular weight distribution (MWD).[30] Therefore, we chose this catalyst system to obtain well-defined glycostars. Table 1 represents the results of the synthesis of glycostars using the silsesquioxane-based macroinitiator and MAIGlc as the monomer. The aim of our study was to obtain well-defined glycostars of different arm lengths. Hence the polymerization was restricted to low conversions to avoid

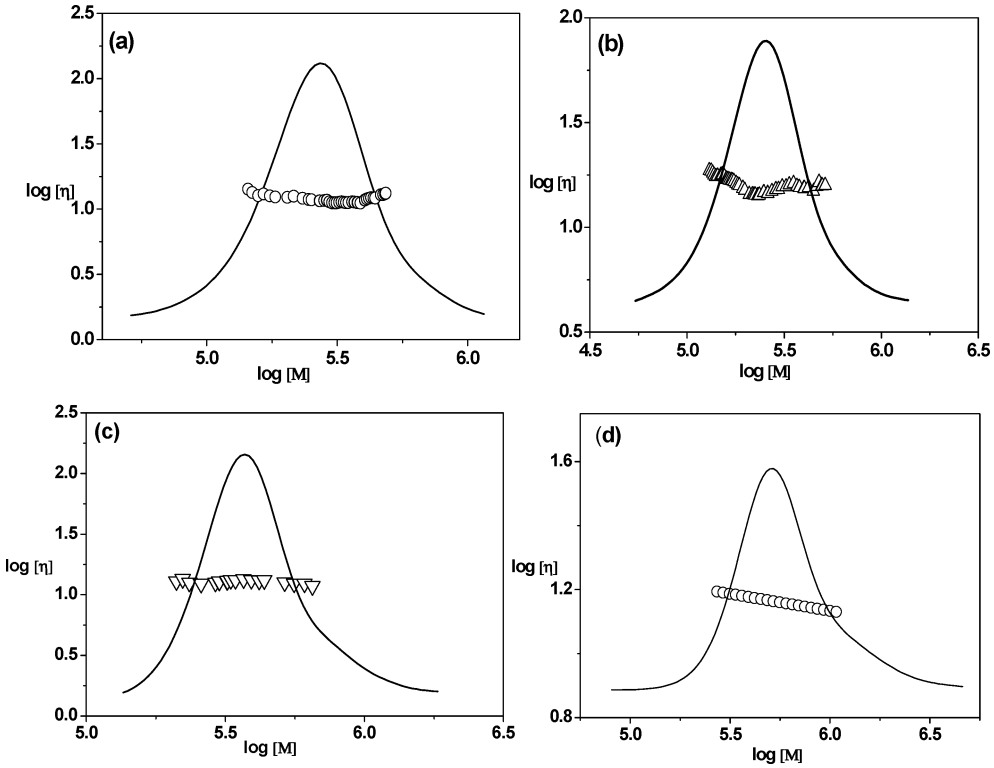

Figure 5. Molecular weight distributions (RI signal) and intrinsic viscosities of (a) glycostar 1, (b) glycostar 2, (c) glycostar 3, and (d) glycostar 4.

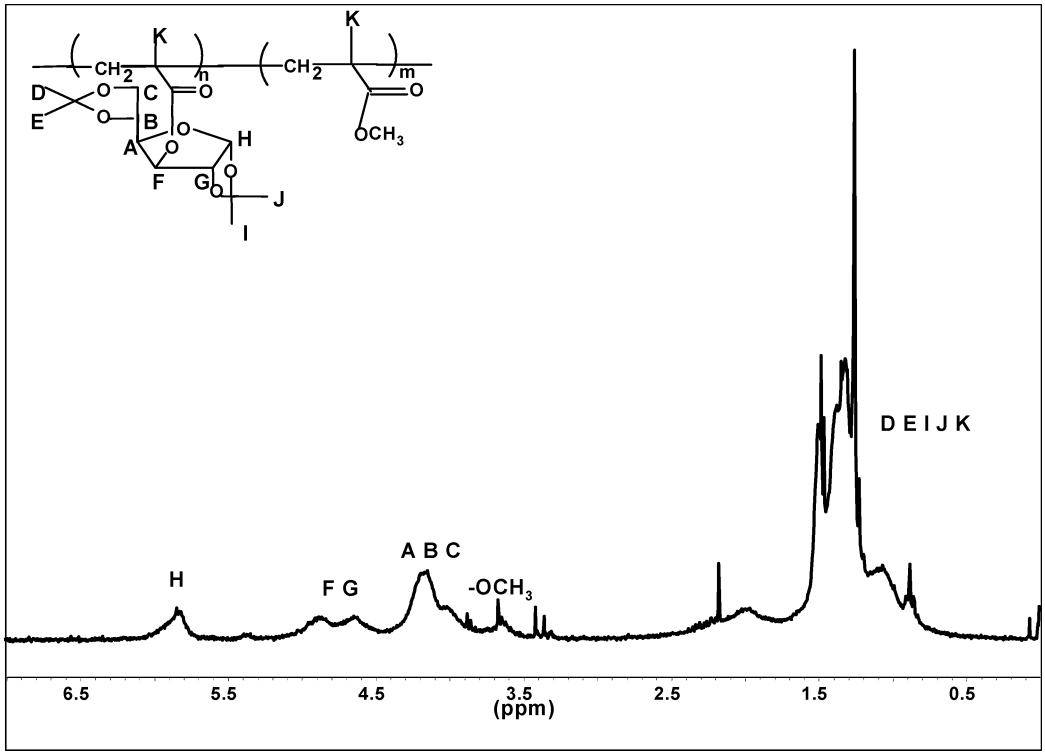

Figure 6. ^{1}H NMR spectrum ($CDCl_3$) of cleaved arms of glycostar 4.

intermacromolecular coupling reactions. As can be seen from Table 1, a high ratio of monomer to initiator and a low conversion were found to be sufficient to suppress undesirable side reactions. It has also been reported by Laine et al. that well-defined eight-arm PMMA stars could be synthesized using octafunctional cubic silsesquioxanes only at very low conversions.[20]

Figure 4 represents the ^{1}H NMR of the glycostar poly(MAIGlc). As can be seen from Figure 4, after the formation of the star with the silsesquioxane core, the characteristic peaks at 1.2−1.4 ppm (isopropylidene protons), 3.8−5.0 ppm, and 5.7−6.0 ppm are clearly seen, indicating the successful formation of the glycostars with silsesquioxane core.

The molecular weights of the resulting glycostars were first estimated by conventional GPC using PtBMA calibration. The GPC traces show monomodal distributions indicating the well-defined and controlled synthesis of the required glycostars as shown in Figure S-1 (Supporting Information). The polydispersities of the polymer samples measured in this study remain low ($M_w/M_n \leq 1.25$, Table 1). The molecular weights obtained by conventional GPC using PtBMA calibration are just apparent ones due to the compact nature of the branched macromolecules and the lack of suitable standards. Hence, GPC/viscosity and GPC/MALS techniques were further used to estimate the true molecular weights of the glycostars.

GPC coupled with an online viscometer (GPC/viscosity) was used to determine the absolute molecular weights as well as the Mark−Houwink exponent for the relationship between intrinsic viscosity and molecular weight of the glycostars. The GPC/viscosity traces exhibit monomodal distributions, as can be seen from Figure 5. The molecular weights obtained by GPC/viscosity are higher than those obtained by conventional GPC using PtBMA calibration, indicating their compact nature (Table 1). The Mark−Houwink exponents will be discussed further below.

The glycostars were further characterized by GPC with a multiangle light scattering detector (GPC/MALS) to obtain the absolute molecular weights and the radii of gyration of the stars. As can be seen from Table 1, the molecular weights are in agreement with those obtained by GPC/viscosity and the calculated ones. The peaks also show monomodal distribution, indicating the well-defined nature of the glycostars. The radii of gyration will be discussed further below.

Arm Cleavage of the Glycostars. To determine the exact initiation site efficiencies, solvolysis of the glycostars with sodium methoxide was performed to cleave the arms from the silsesquioxane core. ^{1}H NMR spectra of the resulting products (cf. Figure 6) revealed that solvolysis of glycostar 4 with sodium methoxide resulted in side chains consisting of a statistical copolymer of 17% MMA and 83% MAIGlc units similar to that observed in the case of the solvolysis of glycocylindrical brushes.[31] The comonomer composition was determined by comparing the peaks at 3.59 ppm attributed to the methyl ester protons (OCH_3) of the MMA units and at 5.8−6.0 ppm attributed to the single ring proton of MAIGlc units. Similar results were obtained for glycostar 3. To calculate the degree of polymerization (DP) of the side chains, the molecular weights of the arms were divided by an average molecular weight of the comonomers, $M_0 = 290$ g/mol.

Table 2 summarizes the detailed characterization of the arms cleaved by solvolysis and the corresponding initiation efficiencies, f. The GPC traces of glycostar 4 and of the cleaved arms are given in Figure 7. The monomodal character of the detached arms shows the absence of inter- and intramolecular coupling reactions. The absolute molecular weights of the cleaved arms were determined by using GPC/MALS measurements. The polydispersity index of the cleaved arms is $M_w/M_n \cong 1.3$ (Table 2), which is a typical value for polymers obtained by slow initiation (limiting $M_w/M_n = 1.33$ for $k_p \gg k_i$ in the Gold distribution[34]). The initiating

Table 2. Characterization of Cleaved Arms of PMAIGlc Glycostars and Initiation Site Efficiencies, f^a

glycostar	$10^{-3}\,M_{n,GPC}{}^b$	$M_w/M_n{}^b$	$10^{-3}\,M_{n,\,GPC/MALS}{}^c$	$DP_{n,calcd}{}^d$	$DP_{n,expt}{}^e$	f (%)
3	20.0	1.28	16.0	23	55.2	42.6
4	27.6	1.38	23.0	35	79.3	44.1

[a] $f = DP_{n,calcd}/DP_{n,expt}$. [b] Determined by GPC using THF as eluent with PMMA standards. [c] Determined by GPC/MALS measurement. [d] Calculated from $M_{n,GPC/MALS}$ assuming 100% initiation site efficiency. [e] Determined by GPC/MALS measurement of cleaved arms after solvolysis.

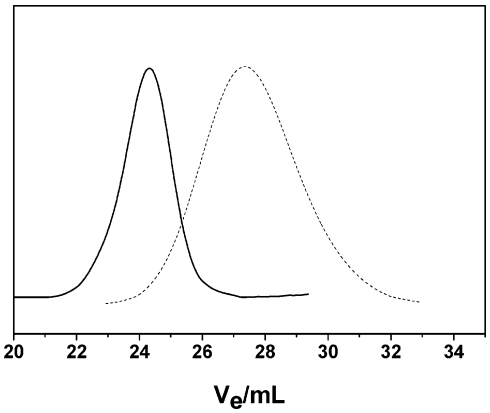

Figure 7. GPC traces of glycostar 4 (—) and cleaved arms (---) after solvolysis.

efficiencies of glycostars 3 and 4 were found to be 42.6 and 44.1% (Table 2), which are attributed to the steric hindrance exerted by the bulky sugar-carrying monomer used in this study. This implies that approximately 25 ± 8 arms have been initiated instead of 58. Correspondingly, the arms of glycostars 1 and 2 are longer than those calculated by a factor of 1/0.43 = 2.3. Even in the case of a less bulkier monomer, such as *tert*-butyl acrylate, the initiating site efficiency using this silsesquioxane-based macroinitiator is in the range of 60−70%,[35] indicating that not only the steric hindrance of the monomer plays a role. To some extent, the structure of the silsesquioxane-based macroinitiator itself could contribute to the lowering of the initiating efficiency due to the enhanced steric crowding as the chain grows, making some of the initiating sites inaccessible.

Solution Properties of Protected Glycostars. The solution properties of glycostars were characterized using GPC/viscosity, GPC/MALS, and DLS measurements. Compared to their linear analogues with the same molecular weight, star polymers have smaller dimensions leading to a lower intrinsic viscosity. This effect becomes more pronounced with increasing number of arms. For stars with the same arm number but with different arm lengths, the Mark−Houwink exponent of the relation between intrinsic viscosity and molecular weight, $[\eta] = K[M]^{\alpha}$, is the same as for a linear polymer.[36] On the other hand, if the arm length is constant and the arm number varies, the Mark−Houwink exponent can become negative.[37] As can be seen from Table 3 and Figure 5, the α values for the four protected glycostars in THF are found to be slightly negative. On one hand, this could result merely from the hydrodynamic broadening in the columns due to the rather low polydispersities of the polymers. On the other hand, it could also result from a polydispersity in arm numbers. To clarify these points, a mixture of glycostars was injected to get a broader molecular weight distribution which is more given by a polydispersity of arm lengths in this case. The number-average molecular

Table 3. Solution Properties of Silsesquioxane-Based Glycostars Before and After Deprotection in THF and Water, Respectively

glycostar	α^a	$R_g{}^b$	$R_h{}^c$	$\rho = R_g/R_h$
1	−0.210		8.7 ± 0.7	
2	−0.094		9.9 ± 0.4	
3	−0.049	10.7 ± 1.3	10.8 ± 0.8	0.99 ± 0.14
4	−0.090	14.6 ± 0.7	14.0 ± 0.7	1.04 ± 0.06
4[d]		14.4 ± 1.3	11.5 ± 0.6	1.25 ± 0.13

[a] Mark−Houwink exponent as determined by GPC/viscosity measurement. [b] Radius of gyration as determined by GPC/MALS. [c] *z*-average hydrodymic radius at 90° as determined by DLS measurements. [d] After deprotection, characterized in water.

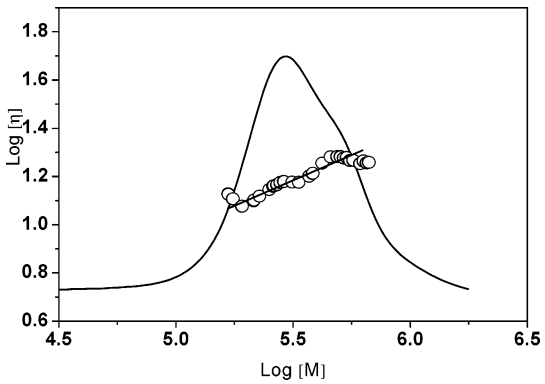

Figure 8. Molecular weight distribution and Mark−Houwink plot for mixture of glycostars 1−4; α = 0.42 ± 0.01.

weight and PDI for the mixture of star polymers are $M_n = 28.3 \times 10^4$ and $M_w/M_n = 1.33$, respectively (Figure 8). The observed Mark−Houwink exponent, α = 0.42 ± 0.01, is close to that (α = 0.51 ± 0.03) for the mixture of linear poly(MAIGlc)s.[30] The slightly lower α value in our study compared to that for the linear poly(MAIGlc)s is attributed to the combined effects of the polydispersity in both the arm number and the arm length in the mixture of glycostars.

The radii of gyration of the glycostars are quite low (Table 3) and increase slightly with the arm length. The Zimm plots are shown in Figure S-2 (Supporting Information). According to Daoud and Cotton,[38] $R_g \sim N^{0.2}M_{arm}{}^{0.5}$; the exponent for the relationship between the molecular weight and radius of gyration, α_s, for the star polymer with constant number of arms is close to that of the corresponding linear polymer. In our study, determination of α_s was impossible owing to the very low radii of gyration (≤15 nm) of the glycostars. Nevertheless, further information was obtained from the combination of GPC/MALS and dynamic light scattering data as described below.

Dynamic light scattering (DLS) was used to determine the hydrodynamic radii of the glycostars in THF solution. Figure 9a shows the normalized intensity correlation functions of glycostar 4 at different angles. The autocorrelation functions were subjected to CONTIN

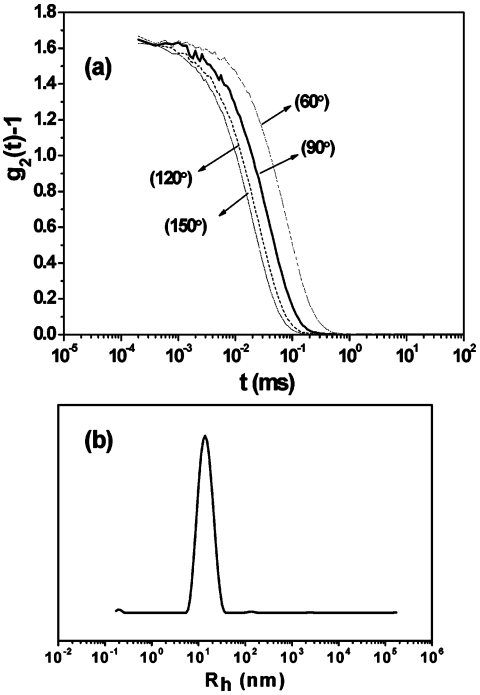

Figure 9. (a) Normalized intensity correlation functions of glycostar 4 in THF at different scattering angles and (b) corresponding intensity-weighted hydrodynamic radius distribution at scattering angle of 90°; $\langle R_h \rangle_z = 14.0$ nm.

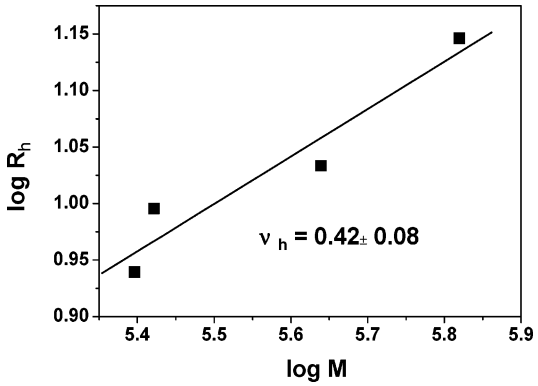

Figure 10. Dependence of hydrodynamic radius on molecular weight of the glycostars.

analysis. The hydrodynamic radius distribution of this brush at a scattering angle of 90° in THF is shown in Figure 9b. Table 3 shows the *z*-average hydrodynamic radius of all glycostars at 90°. The angular dependence of the hydrodynamic radii is very low, as expected for spherical structures. A structure-sensitive parameter is obtained from the ratio, $\rho = R_g/R_h$. As can be seen from Table 3, this parameter is close to unity. It has been calculated by Burchard et al.[2] that, for star molecules with monodisperse arms and $f \gg 1$, $\rho = 1.079$ under θ-conditions.

Figure 10 shows the molar mass dependence of the hydrodynamic radius (the radii of gyration of stars 1 and 2 were too low to allow for a reliable measurement, but the ratio R_g/R_h apparently is constant). As mentioned earlier, for the star polymer with constant number of arms, the exponent should be close to that of the corresponding linear polymer. In our study, the value of $\nu_h = 0.42 \pm 0.08$ is slightly lower than 0.5 but is close to the observed Mark−Houwink exponent, $\alpha = 0.42 \pm 0.01$, for a mixture of star polymers. This lower

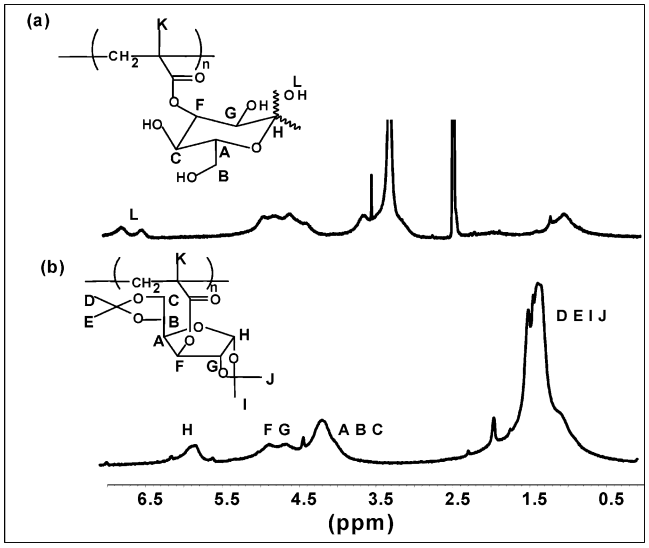

Figure 11. ^{1}H NMR spectra of (a) deprotected glycostar 4 with MAGlc arms (DMSO-d_6) and (b) glycostar 4 with MAIGlc arms ($CDCl_3$).

value again indicates the slight polydispersity in both the arm number and the arm length.

The structures of these glycostars were further visualized using scanning force microscopy (SFM) and scanning electron microscopy (SEM) (see below).

Deprotection and Solution Properties of Deprotected Glycostars. Water-soluble glycostars were obtained by deprotection of the isopropylidene groups by treating the samples with formic acid at room temperature.[30] Figure 11a represents the ^{1}H NMR spectrum of the deprotected glycostar 4. The signals of the isopropylidene protons (1.2−1.4 ppm) completely disappear and a broad signal due to the anomeric hydroxyl groups of the sugar moieties (6.4−7.0 ppm) appears, indicating the quantitative deprotection of the isopropylidene groups. These stars are completely soluble in water and methanol, but are insoluble in THF, chloroform, and hexane.

DLS was performed to study the solution properties of the deprotected glycostar 4 in water. The CONTIN analysis of the autocorrelation functions showed a bimodal hydrodynamic radius distribution with R_h = 11.5 and 88 nm, respectively. The hydrodynamic radius distribution at a scattering angle of 90° in water is shown in Figure 12. The values of R_h for the smaller species are independent of the scattering angle, whereas those for the larger species show a pronounced angular dependence, indicating the formation of polydisperse aggregates that could be due to hydrogen-bonding interactions between the hydroxyl groups. Although these large species contribute considerably to the intensity of the scattered light, their weight or even mole fraction seems to be vanishing (less than a few percent by weight) and hence their presence in the system may be neglected.

The deprotected glycostar 4 was further characterized by asymmetric flow field-flow fractionation (AF-FFF) with a MALS detector in water with 25 mM $NaNO_3$, which was added to minimize the interaction of the polymer with the membrane. As can be seen from Figure 13, there are two species separated by the cross-flow under the conditions used for elution. The amount of the first species is very low, as can be seen from the concentration signal, and is almost absent in the MALS

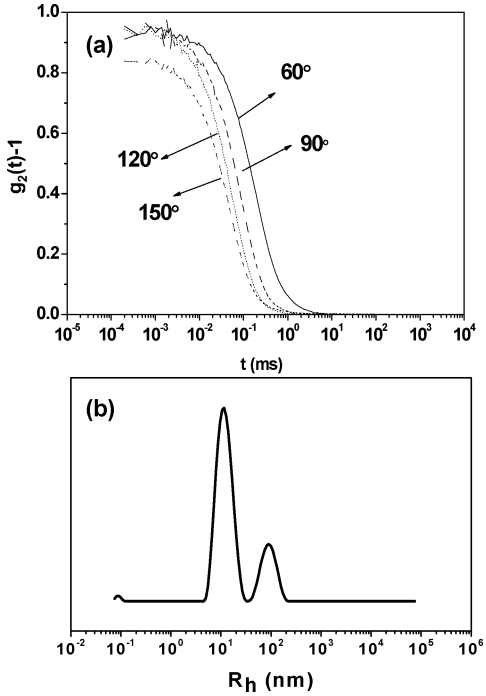

Figure 12. (a) Normalized intensity correlation functions at different scattering angles and (b) corresponding intensity-weighted hydrodynamic radius distribution at scattering angle of 90° of deprotected glycostar 4 in water (0.5 g/L).

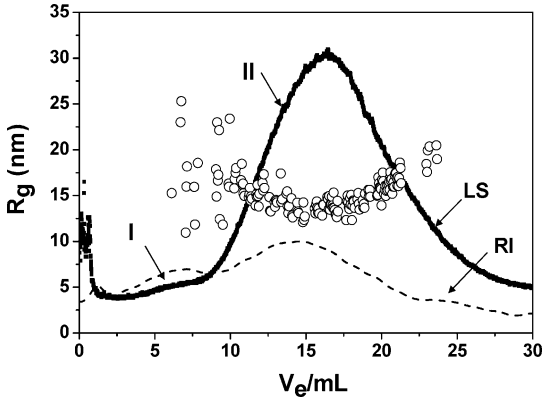

Figure 13. Asymmetric flow field-flow fractionation (AF-FFF/MALS) traces of deprotected glycostar 4 in water (0.5 g/L) with 25 mM $NaNO_3$ and (—) radius of gyration at a scattering angle of 90°.

signal. The molecular weight and PDI for the first species (area I in Figure 13) are found to be $M_n \sim 29 \times 10^4$ and $M_w/M_n = 1.22$, which could to due to a small population of stars with smaller arm lengths (DP ~ 47) or lower arm number (~15). The radius of gyration is too low to be determined for the first species. The molecular weight and PDI of the second species (area II), which is the required deprotected glycostar 4, are determined to be $M_n = 53.5 \times 10^4$ ($M_{n,calcd} = 49.2 \times 10^4$) and $M_w/M_n = 1.16$, respectively. The radius of gyration is ~14 nm, which is quite comparable to that before hydrolysis (14.6 nm). The Zimm plot for the deprotected glycostar 4 is shown in Figure S-3 (Supporting Information). The structure-sensitive parameter, ρ, for the deprotected glycostar 4 is found to be $\rho = 1.25 \pm 0.13$, which is slightly but not significantly higher than the value obtained before hydrolysis. The increase in the ρ value after hydrolysis might be attributed to excluded volume interactions that have been predicted to increase the ρ values by around 13−17% in simulations.[39−41] There is no significant peak for aggregates as was seen in DLS, which shows that the presence of aggregates in our system may be neglected.

The deprotected glycostar 4 was further visualized by SFM and FE-SEM as decscribed in the next section.

Visualization of the Glycostar/Silsesquioxane Hybrids by Scanning Force and Electron Microscopies. Protected Glycostars. To obtain further insight into the morphology of these hybrid glycostars, they were characterized by scanning force microscopy (SFM) by spin-coating a very dilute THF solution (8 mg/L) onto a freshly cleaved mica sheet. Figure 14 displays an image of glycostar 4. Spherical isolated particles are clearly seen, indicating the uniform and well-defined formation of hybrid stars. The diameter of the particle marked by a rectangle in Figure 14a is 46 nm (noncorrected for the tip radius), and the height is ~5 nm (see Figure S-4, Supporting Information), which is somewhat higher than the diameter of the starting silsesquioxane nanoparticles (~3 nm). The polymer/silsesquioxane hybrids are much larger in diameter than the starting material, but very flat, indicating the collapsed structure of the hybrids on mica. Since the diameter obtained by SFM is always too high due to the tip size convolution, field emission scanning electron microscopy (FE-SEM) measurements were performed to obtain the exact size of the resulting glycostar hybrids.

Figure 15 displays the FE-SEM image of glycostar 4, prepared by spin-coating from a dilute THF solution (8 mg/L) onto a silicon wafer. Well-defined and isolated particles can be clearly seen. The average diameter of these glycostars varies between 28 and 31 nm. This value is quite comparable to the results obtained by GPC/MALS and DLS ($R_g = 14.6$ nm and $R_h = 14$ nm, respectively). Hence these results confirm the successful formation of glycopolymer/silsesquioxane hybrid stars.

Deprotected Glycostars. Figure 16 shows an SFM image of the deprotected glycostar 4, spin-coated from a water−methanol mixture (volume ratio of 1/1) onto a freshly cleaved mica sheet. Spherical isolated particles are seen like those before hydrolysis, indicating that the structures of the glycostars are retained during hydrolysis. The cross-section of the particle marked in Figure 16b is shown in Figure S-5 (Supporting Information), and the diameter is found to be 40 nm. The height is ca. 3 nm, similar to the starting nanoparticles, indicating an even more collapsed structure. The diameters vary between 35 and 40 nm, but these values again suffer from convolution with the tip size.

FE-SEM images were taken for deprotected glycostar 4 after spin-coating the sample from water−methanol mixture (volume ratio of 1/1) onto a silicon wafer. As can be seen from Figure 17, there are isolated spherical objects of sizes ranging from 30 to 40 nm. Unlike the SFM images, some huge aggregates of approximately 100 nm in diameter are seen. This mainly could be due to the different substrates used for SFM and FE-SEM in the present study. In the case of silicon substrate, probably the interaction between the deprotected stars is much stronger than that with the substrate, resulting in the formation of aggregates during drying. The aggregates appear to have formed by the combination of several isolated particles. Nevertheless, the size of the deprotected glycostar 4 (diameter = 30−40 nm) is quite comparable to that obtained by AF-FFF and DLS measurements ($R_g = 14.4$ nm and $R_h = 11.5$ nm, respectively).

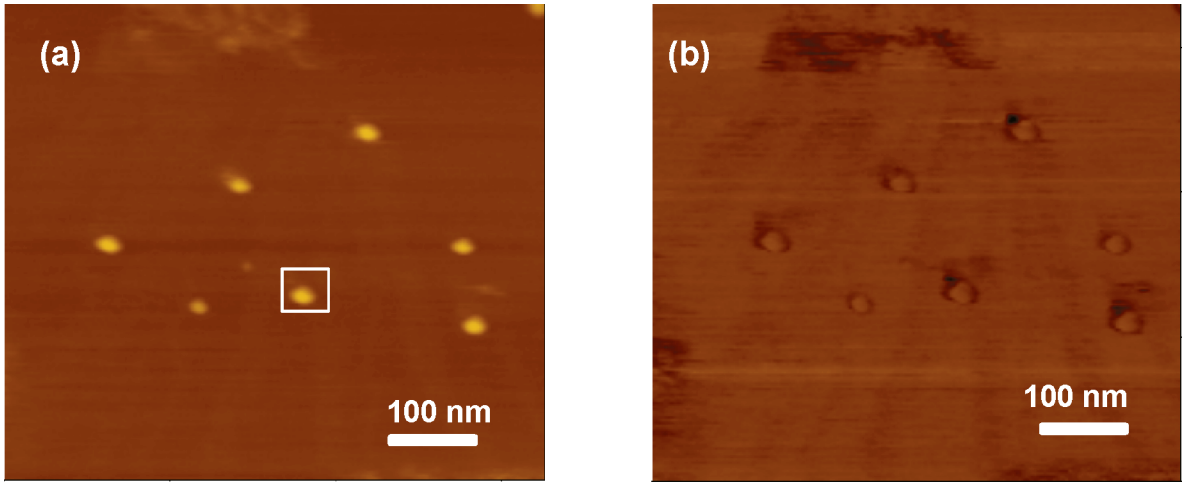

Figure 14. SFM tapping mode images of glycostar 4, spin-coated from dilute THF solution onto mica: (a) height image (z-range, 20 nm) and (b) phase image (range, 45°).

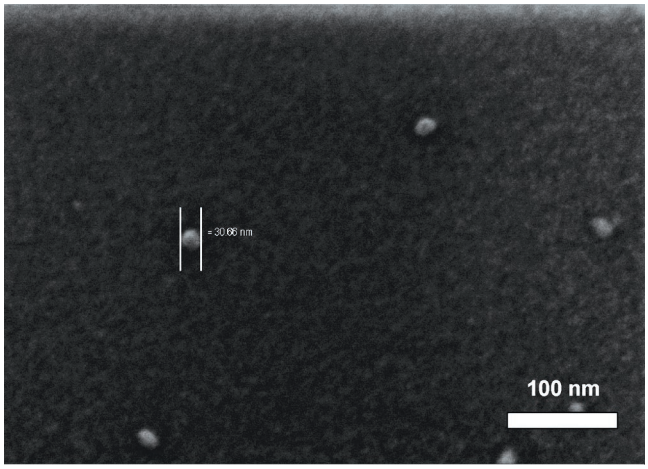

Figure 15. Representative FE-SEM image of glycostar 4, spin-coated from dilute THF solution onto a silicon wafer.

The structure of the deprotected glycostar 4 was further characterized using cryo-TEM and TEM (negative staining using uranyl acetate) in aqeuous solution. Cryo-TEM allows direct imaging of the original shape and size of the polymers in solution, since the sample is vitrified before the measurement. As can be seen from Figure 18, cryo-TEM shows small dots which denote only the silsesquioxane-based core of the stars and the diameter is approximately 5 ± 2 nm. The shell is not seen in the cryo-TEM image due its very low contrast against water. To get further insights, TEM images were recorded using negative staining with uranyl acetate, which is shown in the inset in Figure 18. Now the contrast mechanism is different and spherical objects are observed similar to those seen from FE-SEM and SFM images. The particle size varies between 25 and 45 nm, and the shell is seen without a distinct core unlike in the case of cryo-TEM.

Conclusions

Functional silsesquioxane nanoparticles could be transformed into a macroinitiator of approximately 58 functions suitable for the successful synthesis of well-defined glycopolymer/silsesquioxane hybrid stars. Analysis of the arms cleaved by basic solvolysis indicated that the initiation site efficiency of the silsesquioxane-based macroinitiator is about 44%, which could be due to the bulkiness of the monomer, MAIGlc, as well as the influence of the structure of the macroinitiator, some

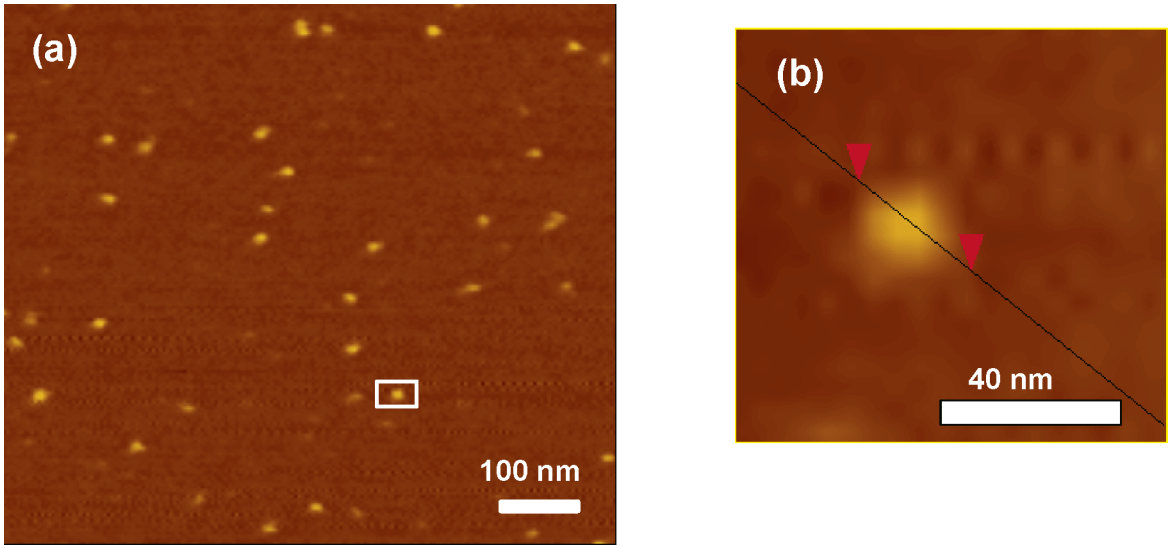

Figure 16. SFM tapping mode images of deprotected glycostar 4, spin-coated from dilute water/methanol (1/1) solution onto mica: (a) height image (z-range, 10 nm) and (b) higher magnification of a single particle marked by a rectangle in (a).

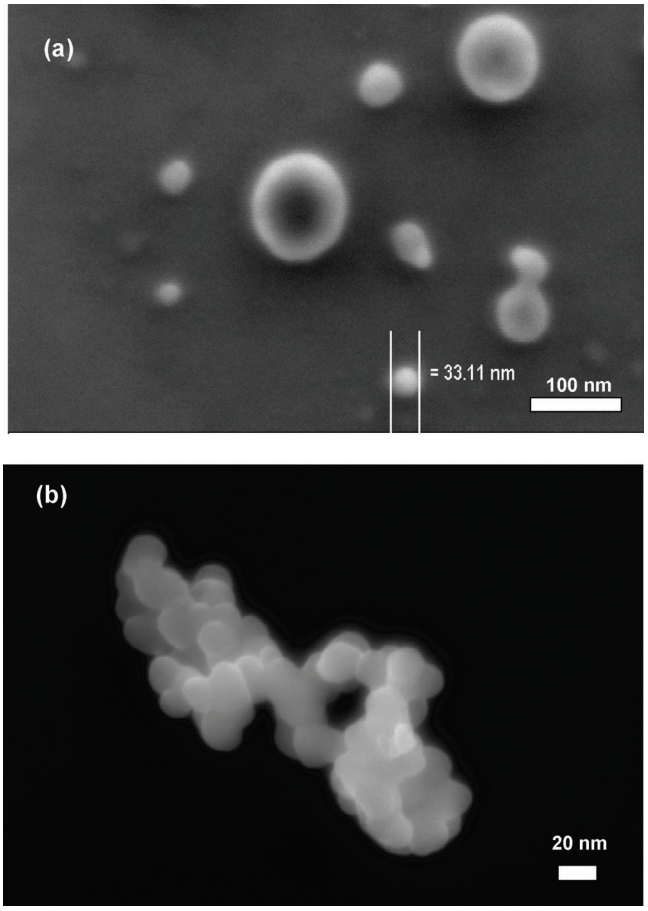

Figure 17. Representative FE-SEM images of (a) deprotected glycostar 4 and (b) aggregate formation, spin-coated from dilute water/methanol (1/1) solution onto a silicon wafer.

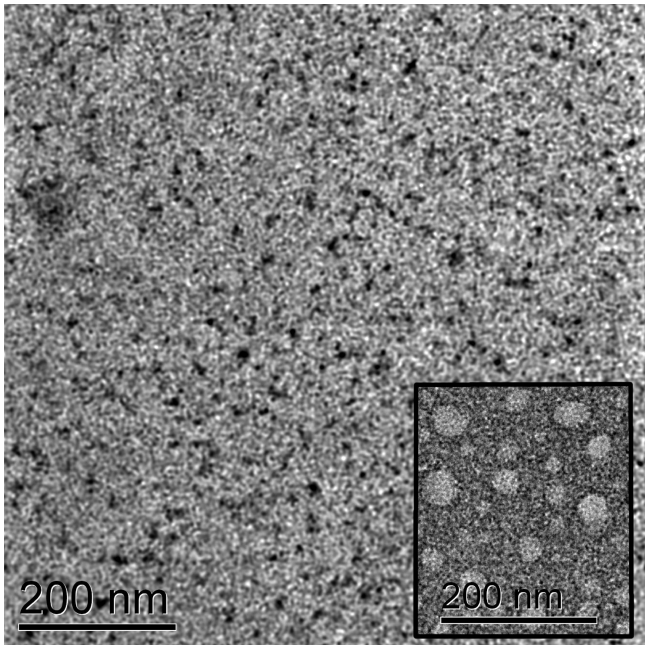

Figure 18. Cryo-TEM image of deprotected glycostar 4. Inset: TEM image obtained by negative staining.

functions possibly being less accessible than others. The absence of inter- or intramolecular coupling reactions was also shown by the unimodal character of the cleaved arms. Both the protected and deprotected glycostars have a spherical structure in THF and water solution, respectively, the various methods resulting in comparable sizes. Those obtained after deprotection have similar shapes and sizes. However, both in DLS and in SEM a tendency for aggregation is seen for the water-soluble glycostars, indicating hydrogen-bonding interactions between the stars.

Acknowledgment. This work was supported by the Deutsche Forschungsgemeinschaft (Grant Mu 896/14). We thank Clarrisa Abetz and Dr. Markus Drechsler for SEM and TEM measurements as well as Sabine Wunder and Evis Penott-Chang for AF-FFF measurements.

Supporting Information Available: Figure S-1, GPC traces; Figures S-2 and S-3, Zimm plots; Figures S-4 and S-5, cross-section analyses. This material is available free of charge via the Internet at http://pubs.acs.org.

References and Notes

(1) Roovers, J. *Encycl. Polym. Sci. Eng.* **1985**, *2*, 478−499.
(2) Burchard, W. *Adv. Polym. Sci.* **1999**, *143*, 113−194.
(3) Hadjichristidis, N.; Guyot, A.; Fetters, L. J. *Macromolecules* **1978**, *11*, 668−672.
(4) Morton, M.; Helminiak, T. E.; Gadkary, S. D.; Bueche, F. *J. Polym. Sci.* **1962**, *57*, 471−482.
(5) Schappacher, M.; Deffieux, A. *Macromolecules* **1992**, *25*, 6744−6751.
(6) Angot, S.; Murthy, K. S.; Taton, D.; Gnanou, Y. *Macromolecules* **1998**, *31*, 7218−7225.
(7) Sawamoto, M. *Plast. Eng. (N.Y.)* **1996**, *35*, 381−436.
(8) Sawamoto, M. *Cationic Polymerizations*; Matyjaszewski, K., Ed.; Marcel Dekker: New York, 1996; p 381.
(9) Hsieh, H. L.; Quirk, R. P. *Anionic Polymerization*; Marcel Dekker: New York, 1996.
(10) Risse, W.; Wheeler, D. R.; Cannizzo, L. F.; Grubbs, R. H. *Macromolecules* **1989**, *22*, 3205−3210.
(11) Simms, J. A. *Rubber Chem. Technol.* **1991**, *64*, 139−151.
(12) Wang, J.-S.; Greszta, D.; Matyjaszewski, K. *Polym. Mater. Sci. Eng.* **1995**, *73*, 416−417.
(13) Wang, J.-S.; Matyjaszewski, K. *J. Am. Chem. Soc.* **1995**, *117*, 5614−5615.
(14) Xia, J.; Zhang, X.; Matyjaszewski, K. *Macromolecules* **1999**, *32*, 4482−4484.
(15) Ohno, K.; Wong, B.; Haddleton, D. M. *J. Polym. Sci., Part A: Polym. Chem.* **2001**, *39*, 2206−2214.
(16) Heise, A.; Hedrick, J. L.; Trollss, M.; Miller, R. D.; Frank, C. W. *Macromolecules* **1999**, *32*, 231−235.
(17) Ueda, J.; Kamigaito, M.; Sawamoto, M. *Macromolecules* **1998**, *31*, 6762−6768.
(18) Matyjaszewski, K.; Miller, P. J.; Pyun, J.; Kickelbick, G.; Diamanti, S. *Macromolecules* **1999**, *32*, 6526−6535.
(19) Plamper, F.; Becker, H.; Lanzendörfer, M.; Patel, M.; Wittemann, A.; Ballauff, M.; Müller, A. H. E. *Macromol. Chem. Phys.* **2005**, *206*, 1813−1825.
(20) Costa, R. O. R.; Vasconcelos, W. L.; Tamaki, R.; Laine, R. M. *Macromolecules* **2001**, *34*, 5398−5407.
(21) Matyjaszewski, K.; Miller, P. J.; Fossum, E.; Nakagawa, Y. *Appl. Organomet. Chem.* **1998**, *12*, 667−673.
(22) Zanini, D.; Roy, R. *J. Org. Chem.* **1998**, *63*, 3486−3491.
(23) Bovin, N. V.; Gabius, H. J. *Chem. Soc. Rev.* **1995**, *24*, 413.
(24) Dordick, J. S.; Linhardt, R. J.; Rethwisch, D. G. *CHEMTECH* **1994**, *24*, 33−39.
(25) Muthukrishnan, S.; Jutz, G.; André, X.; Mori, H.; Müller, A. H. E. *Macromolecules* **2005**, *38*, 9−18.
(26) Narain, R.; Armes, S. P. *Chem. Commun.* **2002**, 2776−2777.
(27) Ohno, K.; Tsujii, Y.; Fukuda, T. *J. Polym. Sci., Part A: Polym. Chem.* **1998**, *36*, 2473−2481.
(28) Mori, H.; Lanzendörfer, M. G.; Müller, A. H. E.; Klee, J. E. *Macromolecules* **2004**, *37*, 5228−5238.
(29) Mori, H.; Müller, A. H. E.; Klee, J. E. *J. Am. Chem. Soc.* **2003**, *125*, 3712−3713.
(30) Muthukrishnan, S.; Mori, H.; Müller, A. H. E. *Macromolecules* **2005**, *38*, 3108−3119.
(31) Muthukrishnan, S.; Zhang, M.; Burkhardt, M.; Drechsler, M.; Mori, H.; Müller, A. H. E. *Macromolecules* **2005**, *38*, 7926−7934.
(32) Neugebauer, D.; Sumerlin, B. S.; Matyjaszewski, K.; Goodhart, B.; Sheiko, S. S. *Polymer* **2004**, *45*, 8173−8179.
(33) Harris, J. R.; Horne, R. W. *Micron* **1994**, *25*, 5−13.

(34) Gold, L. *J. Chem. Phys.* **1958**, *28*, 91.
(35) Plamper, F.; Müller, A. H. E. Unpublished results.
(36) Roovers, J.; Zhou, L. L.; Toporowski, P. M.; Vanderzwan, M.; Iatrou, H.; Hadjichristidis, N. *Macromolecules* **1993**, *26*, 4324−4331.
(37) Held, D.; Müller, A. H. E. *Macromol. Symp.* **2000**, *157*, 225−237.
(38) Daoud, M.; Cotton, J. P. *J. Phys.* **1982**, *43*, 531−538.
(39) Rey, A.; Freire, J. J.; de la Torre, J. G. *Macromolecules* **1987**, *20*, 342.
(40) Freire, J. J.; Rey, A.; Delatorre, J. G. *Macromolecules* **1986**, *19*, 457−462.
(41) Freire, J. J.; Pla, J.; Rey, A.; Prats, R. *Macromolecules* **1986**, *19*, 452−457.

MA051949E